Dependences of the divertor and midplane heat flux widths in NSTX

T.K. Gray1,2), R. Maingi 2), A.G. McLean 2), V.A. Soukhanovskii 3) and J-W. Ahn 2)

1) Oak Ridge Institute for Science and Education (ORISE), Oak Ridge TN USA
2) Oak Ridge National Laboratory, Oak Ridge TN USA
3) Lawrence Livermore National Laboratory, Livermore CA USA

E-mail contact of main author: tkgray@pppl.gov

Abstract. We report the dependence of the lower divertor surface heat flux profiles, measured from infrared thermography and mapped magnetically to the midplane on loss power into the scrape-off layer (P_{LOSS}), plasma current (I_P), and magnetic flux expansion (f_{exp}), as well as initial results with lithium wall conditioning in NSTX. Here we extend previous studies [R. Maingi et al, J. Nucl. Mater. **363–365** (2007) 196–200] to higher triangularity ~ 0.7 and higher $I_p \leq 1.2$ MA. First we note that the mapped, midplane heat flux width, λ_q^{mid}, is largely independent of P_{LOSS} for $P_{LOSS} \geq 4$ MW. λ_q^{mid} is also found to be relatively independent of f_{exp} at 0.8 – 1 cm; peak heat flux is strongly reduced as f_{exp} is increased, as expected. Finally, λ_q^{mid} is shown to strongly contract with increasing I_p such that $\lambda_q^{mid} \propto I_p^{-1.6}$ with a peak divertor heat flux of $q_{div,\,peak} \sim 15$ MW/m^2 when I_p = 1.2 MA and $P_{LOSS} \sim 6$ MW. These scalings are used to project the divertor heat flux for the planned NSTX-Upgrade, with heating power between 10 — 15 MW, B_t = 1.0 T and I_p = 2.0 MA.

1. Introduction

Spherical tori (ST) face the prospect of high heat flux onto the plasma facing components (PFC), owing to their compact nature and design as high power density systems. The divertor heat flux profile and its characteristic scale length, λ_q^{div} are determined by the balance of parallel and perpendicular thermal transport in the scrape-off layer (SOL), along with volumetric losses along the open field lines. Near term research in this area at the National Spherical Torus Experiment (NSTX) [1] has been motivated in part by U.S. DoE multi-machine Joint Research Milestone in 2010, which seeks to understand thermal transport in the SOL through experiments on Alcator C-Mod, DIII-D and NSTX. In addition, the upcoming center stack and neutral beam upgrade on NSTX [2] have motivated further work on understanding the scaling of λ_q^{mid} (where $\lambda_q^{mid} = \lambda_q^{div} / f_{exp}$ and f_{exp} is the magnetic flux expansion) with heating power and plasma current I_p, particularly for highly shaped plasmas.

NSTX has previously measured the dependence of the outer divertor peak heat flux, $q_{div,\,peak}$, on controlled engineering parameters such as I_p and power loss through the scrape-off layer, P_{LOSS} [3][4]; a preliminary assessment of the divertor heat flux widths was also made in these experiments. Here we present systematic analysis of the divertor heat flux widths from both those experiments and new ones, for projection to the planned NSTX-Upgrade. The planned upgrade to NSTX will stress the thermal limits of NSTX's graphite PFCs with neutral beam input power, $P_{NBI} \leq 12$ MW; RF heating power, $P_{RF} \leq 6$ MW; toroidal magnetic field, $B_t \leq$ 1T; $I_p \leq 2$ MA; and pulse lengths up to 5 sec. Viable divertor designs may require some combination of heat flux mitigation techniques, including some combination of a detached or radiative divertor [5], high magnetic flux expansion [6], and/or a snowflake divertor [7][8].

2. Experimental Apparatus

NSTX is a medium-sized spherical torus with a major radius R = 0.85 m, minor radius, a $\leq$ 0.65 m (R/a $\geq$1.27), $I_p \leq 1.4$ MA, $B_t \leq 0.55$ T, $P_{NBI} \leq 7.4$ MW, $P_{RF} \leq 6$ MW, and pulse lengths

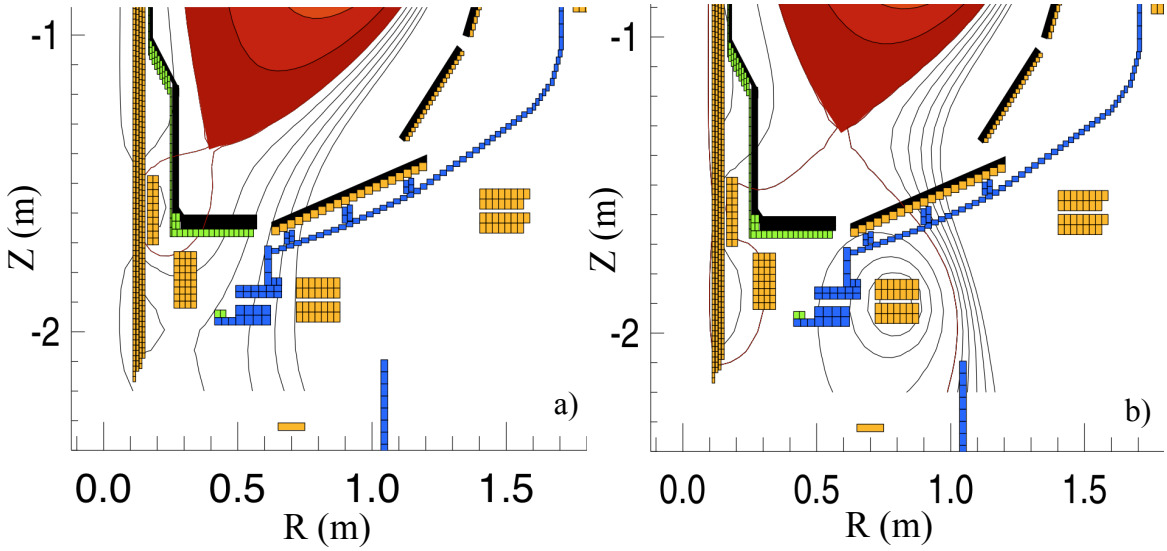

Figure 1: Efit01 equilibrium reconstructions for 2 discharges with different plasma shapes. (a) High δ discharge (shot# 128640, 0.4 s) with δ ~ 0.7, κ = 2.3 and f_{exp} = 16. (b) Low δ discharge (shot# 132341, 0.41 s) with δ ~ 0.44, κ = 2.1 and f_{exp} = 4.

of ≤ 1.8 sec. The NSTX open divertor geometry enables a wide range of discharge shapes, both high and low triangularity (δ) discharge shapes, shown in Figure 1, as well as a range of magnetic flux expansions, f_{exp}.

Surface IR emissivity measurements are captured by an Indigo Omega camera at a 30 Hz frame rate, with surface temperature derived from both an *ex-situ* calibration with a blackbody calibration source and an *in-situ* calibration during vacuum bake-outs [9]. Since 2006 NSTX has employed evaporative lithium wall conditioning on its ATJ graphite plasma facing surfaces during some or all of the run campaign [10]. The key results presented in Sections 3.1—3.3 are for discharges with boronized walls and *not* with lithium wall conditioning. This is because the application of thin lithium films alters the surface emissivity of graphite tiles, and the surface emissivity could be continuously modified due to the chemical reactivity of lithium and the erosion and redeposition of the lithium films during a discharge.

All of the data presented here are for lower single null (LSN), deuterium H-mode discharges, with line averaged electron densities, $\overline{n_e}$ = 4 – 7x10^{19} m^{-3}; B_t ≅ 0.45 T; and the magnetic balance, δ_r^{sep} between 0.005 – 0.015 m. δ_r^{sep} is defined as the radial distance between the upper divertor separatrix flux surface and the lower divertor separatrix flux surface as measured at the outer midplane. Given the 30 Hz frame rate of the IR camera system, measurements obtained are averaged over small edge localized modes (ELMs), which are ubiquitous through out the H-mode phase of the discharges. Time slices just after large transients, disruptions or large Type-I ELMs that result in a large, rapid decrease (≥10%) in the plasma stored energy, W_{MHD}, have been removed.

Figure 2 shows typical discharge parameters along with the measured change in divertor surface temperature, $\Delta T_{div,\ peak}$, and $q_{div,\ peak}$. Heat flux is calculated based on a 1-D, semi-infinite heat conduction approximation [11][12]. The peak divertor temperature rise (Figure 2d) flattens as $\overline{n_e}$ rises continuously through out the discharge. The peak divertor heat flux is reached at ~ 0.35 sec and then decreases as the density rises. However, the power to the

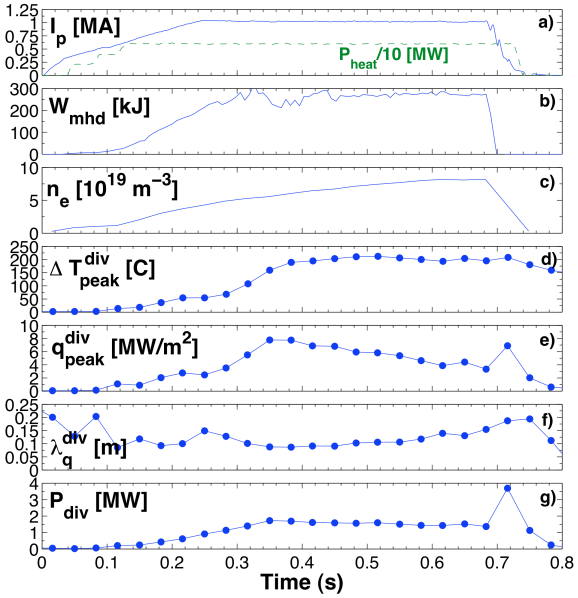

Figure 2: Typical progression of discharge parameters for NSTX (shot# 128640) in a) I_p and P_{heat}, b) plasma stored energy, W_{MHD}, c) $\overline{n_e}$, d) ΔT^{div}_{peak} e) $q_{div,\ peak}$, f) λ^{div}_q and g) power to the outer divertor, P_{div}.

outer divertor remains constant, shown in Figure 2g, after the peak heat flux is reached. This is due to a broadening of the divertor heat flux profile (Figure 2f). Because of the secular $\overline{n_e}$ rise, the data presented are limited to 100 — 200 ms windows after the onset of H-mode and after W_{MHD} has reached steady state. Changes in $\overline{n_e}$ and δ_r^{sep} with in this time window do not appear to affect the width of the heat flux footprint. For example the analysis window for the discharge shown in Figure 2 is from 0.3 – 0.5 s. While this results in a conservative estimate of the heat flux width scaling with respect to the present discharges, future operation in NSTX and NSTX-upgrade should result in steady density profiles. We anticipate execution of experiments with density in the lower range shown in Figure 2c in NSTX-upgrade, and so the projections and divertor designs for NSTX-Upgrade should accommodate such experiments.

3. Results

As described earlier, the measurements obtained are averaged over small ELMs [13], as routinely observed in NSTX discharges with boronized walls. In order to compare results from NSTX to those of other tokamaks, an integral definition of the characteristic scale length, λ^{div}_q of the heat flux is used. While this definition of λ^{div}_q differs from the one used in previous work [3][4], the integral definition facilitates comparison across devices, as was discussed in [14]:

$$\lambda_q^{div} \equiv \frac{P_{div}^{out}}{2\pi R_{div,\ peak}^{out}\, q_{div,\ peak}^{out}}, \qquad (1)$$

where $q^{out}_{div,\ peak}$ is the peak in the divertor heat flux measured from IR thermography, $R^{out}_{div,\ peak}$ is the radial location the peak heat flux occurs, and P^{out}_{div} is the outer divertor power derived from the measured divertor heat flux defined as,

$$P_{div}^{out} = \int_{R_{min}}^{R_{max}} 2\pi R_{div}^{out}\, q_{div}^{out}\, dr, \qquad (2)$$

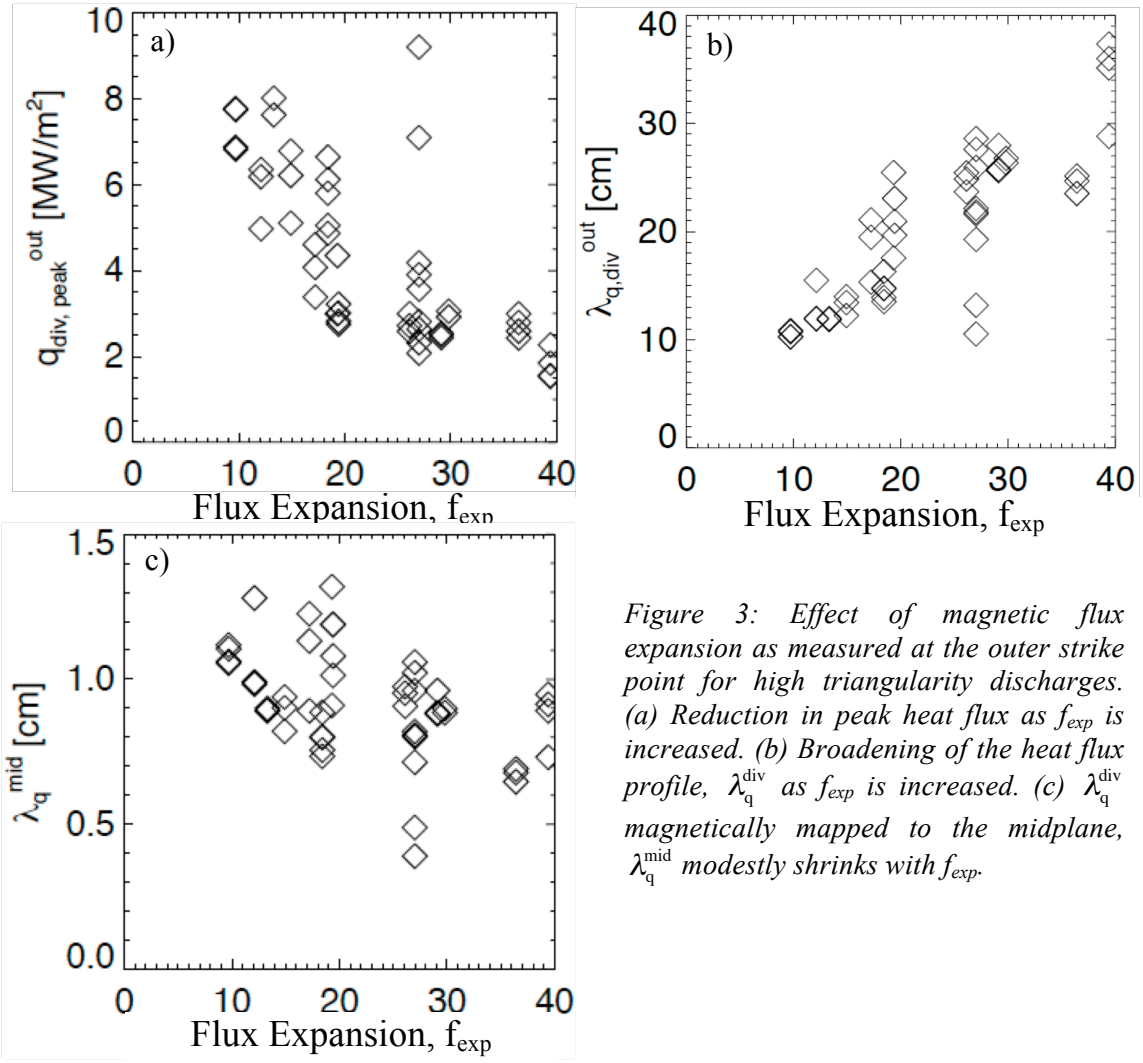

Figure 3: Effect of magnetic flux expansion as measured at the outer strike point for high triangularity discharges. (a) Reduction in peak heat flux as f_{exp} is increased. (b) Broadening of the heat flux profile, λ_q^{div} as f_{exp} is increased. (c) λ_q^{div} magnetically mapped to the midplane, λ_q^{mid} modestly shrinks with f_{exp}.

where R_{min}-$R_{div,\,peak}$ = -0.05 m and R_{max}-$R_{div,\,peak}$ = 0.20 m. λ_q^{div} is then magnetically mapped to the mid-plane such that $\lambda_q^{mid} = \lambda_q^{div} / f_{exp}$, where f_{exp} is the average magnetic flux expansion measured at the outer strike point along the ~ 5 mm midplane flux surface, and defined as $f_{exp} = \left(R_{mid} B_\theta^{mid}\right) / \left(R_{div} B_\theta^{div}\right)$. B_θ^{mid} and B_θ^{div} are the midplane and divertor poloidal magnetic fields at radial locations R_{mid} and R_{div} respectively.

3.1. λ_q^{mid} scaling with Magnetic Flux Expansion

The magnetic flux expansion was varying by changing the x-point height in NSTX. Highly shaped (δ~0.8, elongation, κ ≅ 2.2-2.4), lower single null H-mode discharges were accomplished [6] with I_p = 1.0 – 1.2 MA and P_{NBI} = 6 MW. Figure 3 shows that $q_{div,\,peak}$ is reduced from 8 MW/m^2 to 2 MW/m^2 by increasing f_{exp} from 10 – 40. The reason for this is a broadening of λ_q^{div} shown in Figure 3(b), where λ_q^{div} increases monotonically from 10 to 37 cm as a function of f_{exp}. Note the two outlying data points with high peak heat fluxes, $q_{div,\,peak}$ ≥ 7 MW/m^2, both at f_{exp} ≅ 27, while the majority of the data at similar f_{exp} have $q_{div,\,peak}$ ≤ 4 MW/m^2. These data are included for completeness, as they cannot be directly attributed to any identifiable transient heat load on the divertor such as large Type-I ELMs.

While an increase in divertor radiation could also be responsible for reducing $q_{div,\,peak}$,

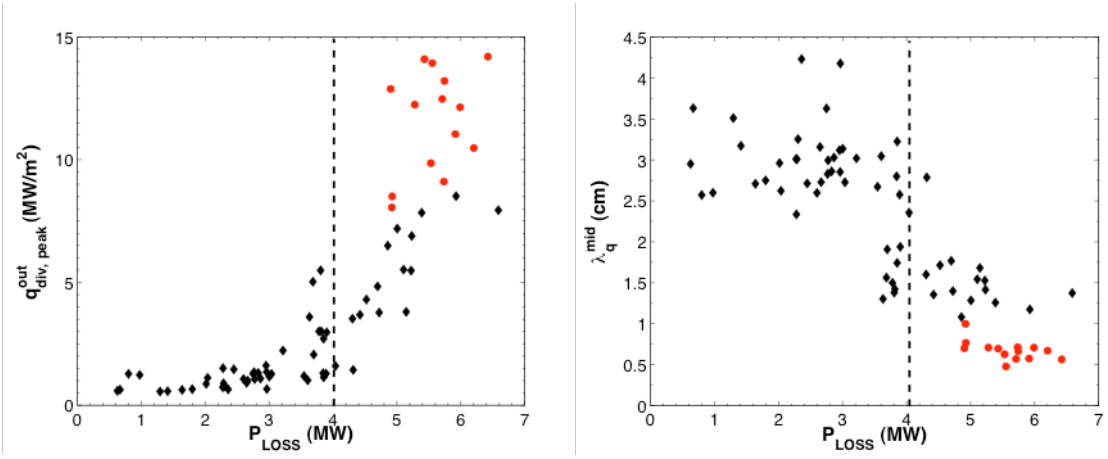

Figure 4: Scan of power lost through the last closed flux surface, P_{LOSS} for low triangularity (◆) and high triangularity (●) discharges. (a) Outer divertor peak heat increasing as P_{LOSS} increases with the change in slope denoted by the vertical dashed line. (b) Reduction in λ_q^{mid} as P_{LOSS} is increased beyond 4 MW suggesting a change in divertor regimes from detached/radiative to attached.

divertor bolometric data are similar for both low and high flux expansion discharges [5]. When λ_q^{div} is magnetically mapped to the midplane as in Figure 3c, the variation in the λ_q^{mid} is 0.95 ± 0.2 cm. Therefore, while $q_{div,peak}$ scales inversely with f_{exp}, the λ_q^{mid} is largely independent of f_{exp}.

3.2. λ_q^{mid} scaling with P_{LOSS}

Figure 4 shows that as P_{LOSS} is increased from 0.5 to 6 MW, the peak heat flux increases as expected. Here P_{LOSS} is defined as $P_{LOSS} = P_{NBI} + P_{oh} - dW/dt - P_{rad}^{core}$, where P_{oh} is the ohmic input power, dW/dt is the time rate of change of the plasma energy, and P_{rad}^{core} is the core radiated power. For low δ discharges (δ ~ 0.5, I_p = 0.8 MA), there is a marked decrease in λ_q^{mid} as P_{LOSS} is increased beyond 4 MW, shifting from an average λ_q^{mid} of approximately 3 cm down to 1.5 cm. This is due to a transition from a radiative (or possibly even partially detached) divertor to an attached, high recycling divertor at P_{LOSS} > 4 MW. The radiated power drops as P_{LOSS} is increased and is consistent with previous 2-point modeling [4][15], where the transition to an attached divertor is denoted by a change in slope of $q_{div,\,peak}$ vs. P_{LOSS} as shown in Figure 4a. We note, however, that a detailed analysis of the divertor regime (as previously done in NSTX [16]) to determine if detachment and volume recombination are occurring has not yet been performed. For the high δ discharges shown in Figure 4b, where δ ~ 0.7, f_{exp} = 16 and I_p = 1.2 MA, λ_q^{mid} is constant at ~ 0.7 cm. Note that, the data for high δ discharges are chosen where $P_{LOSS} \geq 5$ MW. Therefore, λ_q^{mid} appears to vary weakly with P_{LOSS}, when the divertor is in an attached regime. We will show in the next section that this difference in λ_q^{mid} values between low and high δ are actually due to a strong I_p dependence in the data.

3.3. λ_q^{mid} scaling with plasma current

Since the results of the previous two sections showed λ_q^{mid} is largely independent of f_{exp} and

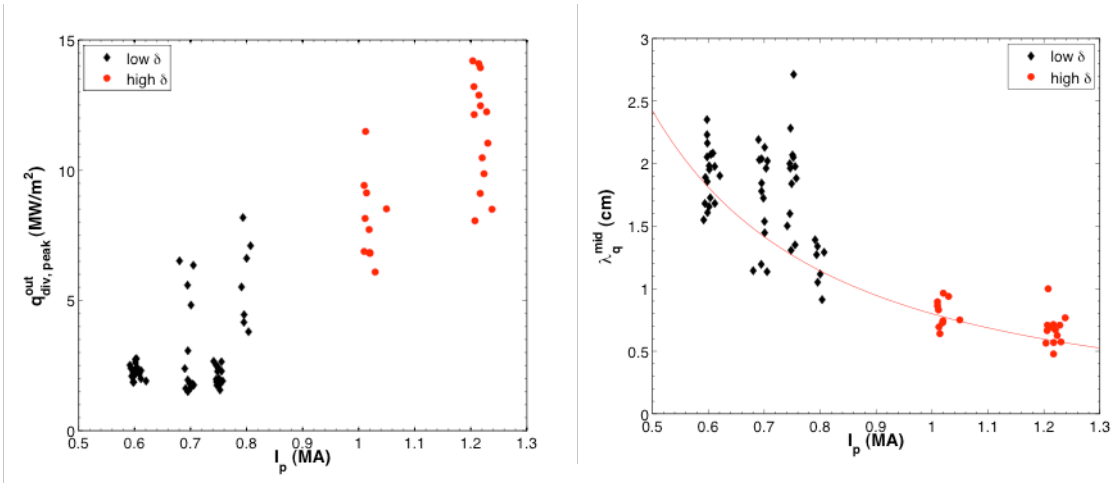

Figure 5: Effect of increasing plasma current, I_p for low triangularity (♦) and high triangularity (•) discharges. (a) Outer divertor peak heat flux increases with increasing plasma current. (b) λ_q^{mid} contracts with increasing plasma curret. (—) Power law fit to the λ_q^{mid} data.

P_{LOSS}, Figure 5 shows that the heat flux and λ_q^{mid} depend on I_p. Here we include low δ discharges (δ ~ 0.5) with P_{NBI} = 4 MW and f_{exp} = 6, as well as high δ discharges (δ ~ 0.7) with f_{exp} = 16 and P_{NBI} = 6 MW. The weak dependences of λ_q^{mid} on other parameters have probably resulted in some of the scatter in Figure 5. Figure 5b shows that λ_q^{mid} strongly contracts with increasing I_p such that $\lambda_q^{mid} = 0.91\, I_p^{-1.6}$. Note that both DIII-D [17] and JET [18] have reported similar trends where λ_q^{mid} is inversely proportional to I_p; DIII-D in particular has reported $\lambda_q^{mid} \propto I_p^{-1.2}$ [19], close to the NSTX result.

Recent simulations of midplane SOL turbulence with the SOLT code [20] were performed for select NSTX discharges. It was concluded that midplane turbulence is the main contributor to the SOL heat flux width for the low power ELM-free H-mode discharges studied, while additional physics is required to explain the strong contraction of λ_q^{mid} with I_p observed experimentally in higher power discharges. One possibility is additional spreading of the heat flux at low I_p as a result of processes in the vicinity of the magnetic X-point.

3.4. Effect of Lithium Wall Conditioning

As previously stated, NSTX has been using lithium for wall conditioning for edge density control, higher confinement times [21], and the elimination of ELMs [22]. The change in surface emissivity due to the lithium coatings makes determining the divertor surface temperature, and therefore the magnitude of the heat flux, questionable with conventional IR thermography. Previous measurements with a single color, slow IRTV system showed that the heat flux profile contracted with lithium wall conditioning [23]. Recently, a two color-IR camera has been developed for NSTX to quantify the heat flux profile with lithium coatings [24]. The system has been designed to be less sensitive to emissivity changes that occur because of the lithium wall conditioning. Figure 6 shows two similar high δ (high f_{exp} ~ 19), 0.8 MA, 4 MW beam heated discharges. Panels a-e show I_p, $\overline{n_e}$, W_{MHD}, D_α and core radiated power, P_{rad}. The non-lithiated discharge (shot# 127975) was taken when NSTX still utilized boronization. While the lithiated discharge (shot# 141256) was taken during the most recent run campaign when only lithium wall conditioning was used. From Figure 6a-c, e it is clear that the discharges evolved in a similar manner. However, Figure 6d shows a nearly

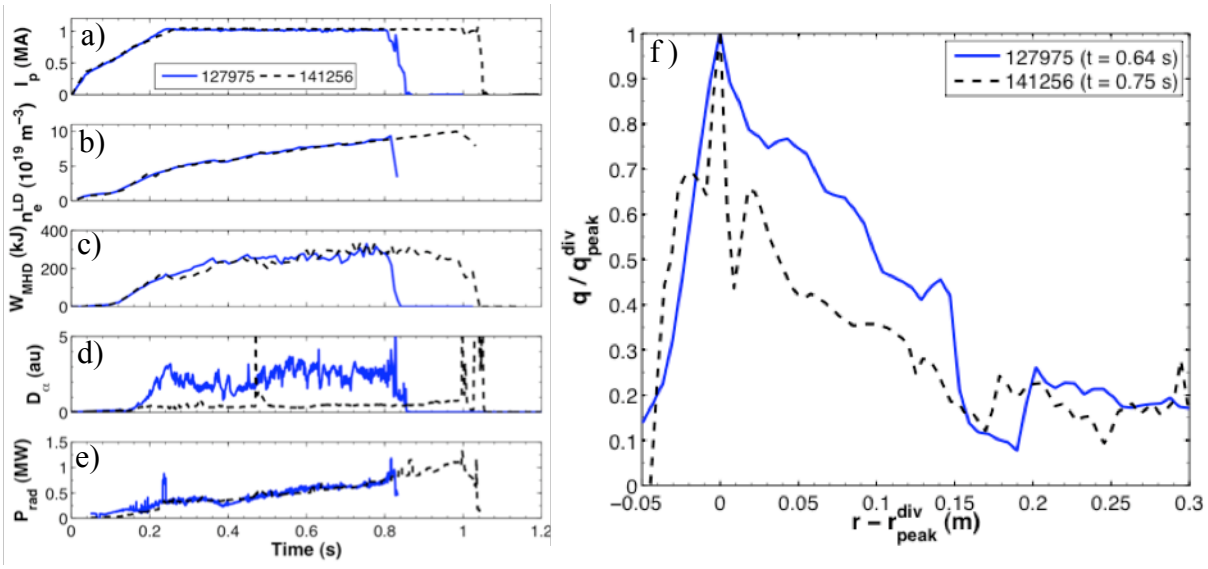

Figure 6: Comparison of two 0.8 MA, high δ, 4 MW beam heated discharges without (—) and with (--) lithium wall conditioning. a) I_p, b) line averaged electron density, c) W_{mhd}, d) lower divertor D_α, e) radiated power, P_{rad}, and f) divertor heat flux profiles taken at t=0.64 and 0.75 sec respectively.

quiescent lower divertor D_α signal for shot# 141256 with lithium. Figure 6f shows the measured divertor heat flux profiles. Measurements for the non-lithium shot were done with the single color, IR system described earlier, while the lithium wall conditioned discharge utilized the new 2-color, fast IR camera system with 50 frames averaged together to yield a similar integration time as the slow IR camera system. From Figure 6f, the λ_q^{div}, as defined by Eq. 1, is found to be 0.249 m with out lithium. However, when lithium wall conditioning is used, λ_q^{div} contracts to 0.0919 m. This is consistent with previous results [23] with single color IR measurements that indicated a 50 – 60% contraction in λ_q^{div} when lithium wall conditioning is employed.

4. Summary and Conclusions

It has been shown that for neutral beam heated, H-mode discharges in NSTX $\lambda_q^{div} \propto f_{exp}$, while $q_{div,\,peak} \propto 1/f_{exp}$. However, when λ_q^{div} is mapped to the midplane, it is relatively independent of f_{exp}. Additionally, λ_q^{mid} is independent of P_{LOSS} in well-attached, high recycling plasmas with high P_{LOSS}. In contrast, λ_q^{mid} is found to vary $\propto I_p^{-1.6}$, with a peak divertor heat flux, $q_{div,\,peak}$ of 15 MW/m^2 reached when I_p = 1.2 MA and P_{NBI} = 6 MW. The I_p scaling covers a wide range of plasma shapes, flux expansions and heating powers. Preliminary analysis of heat flux profiles obtained with the 2-color, fast IR system indicates that the divertor heat flux width, $\lambda_{q,\,lithium}^{div} \approx \frac{1}{2}\lambda_{q,\,non\text{-}lithium}^{div}$ for these discharge conditions. This confirms earlier measurements [23] of λ_q^{div} performed with the single color IR system that showed λ_q^{div} contracts with the addition of lithium wall coatings.

To project for an upgraded NSTX (NSTX-U) [2], Eq. 1 can be re-written to estimate the peak heat flux on the divertor such that $q_{div,\,peak}^{out} = P_{div}^{out} / \left(2\pi R_{div,\,peak}^{out} f_{exp} \lambda_q^{mid}\right)$, where $P_{div}^{out} \approx f_{div} P_{heat}$, f_{div} = 0.5 and $\lambda_q^{mid} \approx 0.9 I_p^{-1.6}$. Therefore, for I_p = 2 MA, P_{NBI} = 12 MW and δ ~ 0.7, the peak

heat flux to the divertor would reach 24 ± 4 MW/m^2 for f_{exp} = 30. It is evident that some technique of heat flux mitigation such as even higher flux expansion, double null operation or radiative/detached divertor operation will be required for NSTX-U as 24 MW/m^2 would exceed the established material limits of ATJ graphite for the 5 sec design pulse lengths. Therefore, understanding λ_q^{mid}'s strong dependence on I_p is the focus of near term theoretical modeling, e.g. neoclassical modeling with the XGC-0 code [25].

Acknowledgements
The authors are grateful to the NSTX research team for diagnostic and technical support. T.K. Gray is supported under an appointment to the U.S. D.O.E. Fusion Energy Postdoctoral Research Program administered by the Oak Ridge Institute for Science and Education under contract number DE-AC05-06OR23100 between the U.S. D.O.E. and Oak Ridge Associated Universities. This research is sponsored by US D.O.E. contracts DE-AC05-00OR22725, DE-AC52-07NA27344, and DE-AC02-09CH11466.

References
[1] M. Ono et al. Nucl. Fusion **40** (2000) 557-561.
[2] J.E. Menard, et al. Proceedings of the 37th EPS Conference on Plasma Phys. (2010)
[3] R. Maingi et al. J. Nucl, Mater. **313-316** (2003) 1005-1009
[4] R. Maingi et al. J. Nucl. Mater. **363–365** (2007) 196–200.
[5] V.A. Soukhanovskii, et al. Phys. Plasmas **16** (2009) 022501
[6] V.A. Soukhanovskii, et al. Nucl. Fusion **49** (2009) 095025
[7] D.D. Ryutov. Phys. Plasmas **14** (2007) 064502
[8] V.A. Soukhanovskii, et al. these proceedings
[9] D.M. Mastrovito et al. Rev. Sci. Instrum. **74**(12) (2003) 5090–5092.
[10] H.W. Kugel et al. Phys. Plasmas. **15** (2008) 056118.
[11] D.N. Hill et al. Rev. Sci. Instrum. **61** (1990) 3548.
[12] C.J. Lasnier et al. Nucl. Fusion. **38** (1998) 1225.
[13] R. Maingi, et al. Nucl. Fusion. **45** (2005) 264.
[14] A. Loarte et al. J. Nucl. Mater. **266-269** (1999) 587–592.
[15] K. Borass et al. Nucl. Fusion **31** (1991) 1035.
[16] V.A. Soukhanovskii et al. J. Nucl. Mater. **337–339** (2005) 475–479.
[17] C.J. Lasnier, Bull. Am. Phys. Soc. (2009)
[18] W. Fundamenski, Private Communication (2009)
[19] C.J. Lasnier et al., submitted to J. Nucl Mater. (2010)
[20] J.R. Myra et al. submitted to J. Nucl Mater. (2010)
[21] M.G. Bell et al. Plasma Phys. Control. Fusion **51** (2009) 124054
[22] R. Maingi et al. Phys. Rev. Lett. **103**(7) (2009) 075001
[23] T.K. Gray, et al. submitted to J. Nucl. Mater (2010)
[24] A.G. McLean et al. submitted to Rev. Sci. Instrum. (2010).
[25] C. S. Chang, et al. Phys. Plasmas **9** (2002) 3884.